Subsonic to Intersonic Transition in Sliding Friction for Soft Solids

Takuya Yashiki,[1] Takehiro Morita,[1,2] Yoshinori Sawae,[1,2] and Tetsuo Yamaguchi[1,2]
[1]Department of Mechanical Engineering, Kyushu University, Fukuoka 819-0395, Japan
[2]International Institute for Carbon-Neutral Energy Research, Kyushu University, Fukuoka 819-0395, Japan

(Received 31 July 2019; revised manuscript received 17 March 2020; accepted 20 May 2020; published 8 June 2020)

We perform friction experiments between a compliant gel and a rigid cylinder at sliding velocities comparable to the Rayleigh wave or secondary wave velocity of the gel. We find that, when the sliding velocity exceeds the wave velocities, the contact state transitions from Hertzian like to flat punch like, resulting in the breakdown of the lubricating oil film and the abrupt increase in the friction coefficient. We succeed in deriving theoretical solutions for the contact pressure distributions and the deformation profiles in the presence of friction, which are consistent with our experimental observations.

DOI: 10.1103/PhysRevLett.124.238001

Sliding friction is a dynamic phenomenon that occurs when two solid bodies are in contact and in relative motion to each other [1]. In normal situations during sliding friction, the sliding velocity V is much smaller than the Rayleigh wave velocity (V_R) or secondary wave velocity (V_S) of the objects [1–16]. In these situations, direct interactions between dry solids [17], fluid films between them [18], and energy dissipation in the bulk [2,19,20] play an essential role in friction. In contrast, if at least one of the frictional pair consists of a soft solid, V becomes comparable to V_R or V_S due to its small elasticity and the inertial effects come into play. These examples can be found when a Formula-1 car applies sudden braking, and when the tire of an aircraft hits the ground upon landing. Similar to what happens when a flying object moves faster than the velocity of sound in air [21], or when the propagation velocity of a shear crack exceeds the secondary wave velocity (called supershear rupture) [22,23], it is highly expected that some specific phenomena like the radiation of shock waves and the generation of Mach cones would be observed during intersonic sliding friction.

In spite of these expectations, however, a limited number of theoretical studies have been reported [24–28]. Their results are summarized as follows: in the case of point contact on a two-dimensional semi-infinite elastic solid (or equivalently, line contact on a three-dimensional solid), steady-state solutions without friction exist for all velocity ranges [24–26,28], and those with friction between V_S and V_P (the primary wave velocity) [27]. However, the expressions in [24] included errors [25–28] and those with friction [27] were proved to be incorrect based on our recalculations, as discussed later. On the other hand, in the case of contact between a rigid cylinder (with a nonzero radius) and an elastic solid, the steady-state solutions without friction exist in the sub-Rayleigh ($V < V_R$) and supersonic ($V > V_P$) regimes [25,26], while the solution for $V_R < V < V_P$ was considered nonphysical, and the effects of friction were not discussed. Thus, the frictional behavior above V_R has not been elucidated in spite of theoretical efforts. Furthermore, very few experiments or numerical simulations have been conducted for transonic regimes and the experimental or numerical evidence presently remains poor. Here we explore the sliding friction of a soft elastic solid against a rigid indenter for these regimes.

In this study, we use silicone gel as a soft solid. It was prepared by mixing and curing the following prepolymers: CY52-276A: CY52-276B: SILPOT184: SILPOT184 CAT (Toray Dow Corning) = 2:8:9:1 (by weight) at 70 °C for 6 h. The shear modulus was measured using a rheometer (MCR-301, Anton-Paar) in an oscillatory shear with a parallel plate (diameter $\phi = 25$ mm). The storage shear modulus G' is 226 ± 2 kPa for frequency ranges from 0.01 to 7.19 Hz, and their loss modulus G'' varies from 1.16 (0.1 Hz) to 3.98 kPa (7.19 Hz). The density ρ is 980 kg/m^3. From these values, the secondary wave velocity of the gel is estimated to be $V_S = \sqrt{G'/\rho} = 15.2$ m/s. The Rayleigh wave velocity V_R is defined by the zero point of the Rayleigh function $R(V)$:

$$R(V_R) = \{2 - (V_R/V_S)^2\}^2 - 4\sqrt{(1 - (V_R/V_P)^2)(1 - (V_R/V_S)^2)} = 0. \quad (1)$$

For an incompressible solid such as rubber or a gel, V_R is much smaller than V_P ($\sim$ km/s). Thus, the calculated Rayleigh wave velocity is $V_R = 0.955 V_S = 14.5$ m/s.

The schematic of the experimental setup is depicted in Fig. 1(a). A gel with a thickness $H = 20$ mm was prepared at the periphery of an aluminum wheel with a radius of 80 mm. Thus, the outer radius R_1 of the gel is 100 mm. The width of the wheel and the gel are $W = 20$ mm. The disk is rotated with a dc motor. A hemicylindrical aluminum indenter with a radius $R_2 = 21$ mm is attached to a

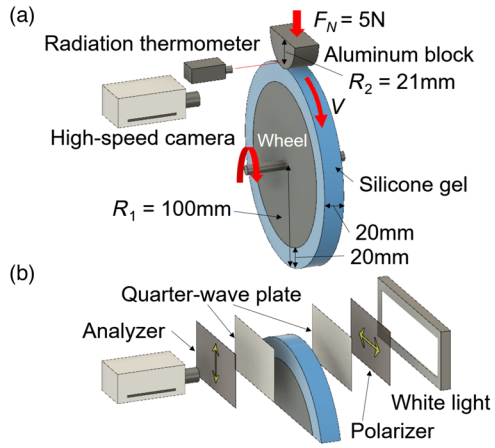

FIG. 1. (a) Schematic of the experimental setup. (b) In photoelasticity experiments, a LED white illumination, a polarizer, an analyzer, and two quarter-wave plates are inserted at the front and back of the sample.

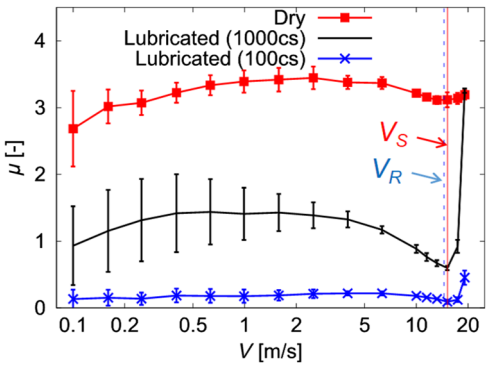

FIG. 2. Sliding velocity—friction coefficient curves for the dry and lubricated (1000 and 100 cs) conditions. The Rayleigh wave and secondary wave velocities are drawn by the blue dotted and red solid lines, respectively.

vertically moving slider and a sliding contact is established from the top of the rotating disk. To reduce the friction, silicone oil ($\nu = 1000$ cSt, KF-96-1000cs, Shin-Etsu Silicone) is used as a lubricant. The sliding velocity V is altered in a stepwise manner every 5 s within the range of 0.1 to 19.1 m/s. The normal load F_N is set to 5 N and the friction force F is measured with a strain gauge attached to the indenter. We calculate the friction coefficient as the average friction force over the middle 3 s for each measurement time, divided by the normal load. We observe the sliding behavior with a high-speed camera (VW-9000, Keyence) at 4000 fps. Furthermore, we perform photoelasticity experiments to visualize the stress distributions inside the gel [see Fig. 1(b)], and estimate the temperature at the frictional interface with a radiation thermometer (IT2-02, KEYENCE) by measuring the temperature of the side face of the aluminum indenter close to the frictional interface (distance < 2 mm).

Figure 2 shows the sliding velocity dependence on the friction coefficient. As a comparison, the results without a lubricant ("Dry") and with silicone oil having a smaller viscosity ($\nu = 100$ cSt, KF-96-100cs, Shin-Etsu Silicone) are also plotted. Regardless of the lubrication conditions, characteristic frictional behaviors can be clearly seen; as the sliding velocity goes up, the friction coefficient gradually increases and then decreases below V_R. In contrast, when the sliding velocity exceeds V_S, it starts to increase and continues to evolve until the maximum sliding velocity is achieved during the experiment ($V = 19.1$ m/s). One possible mechanism for the decrease in friction below V_R is the inertia-induced softening [25,26], which leads to widening of the contact region [see Fig. 5(c)], reduction in the contact pressure, and thickening of the oil film. Another is the reduction in the viscous drag due to the shear thinning of a lubricant. These result in the reduction in friction for lubricated contact; however, it is not evident for dry friction. Further investigations are required to understand the mechanisms.

To understand the mechanisms for the abrupt increase in friction above V_S, we firstly discuss the effect of the interfacial temperature, since a temperature increase might cause a reduction in the viscosity of the silicone oil, loss of the load supporting capacity, and then breakdown of the oil film; thus, leading to a further increase in friction. The time evolution of the measured interfacial temperature is plotted in Fig. 3(a). The temperature starts from room temperature ($\approx$25 °C) and gradually increases below V_R (blue region). As the sliding velocity exceeds V_R (red region), the temperature still shows a gradual increase (though a small jump is recognized just above V_R), and finally exhibits a rapid increase at $V = 19.1$ m/s ($t = 75$ s), which is well above V_R (and V_S). In other words, the critical sliding velocity beyond which the abrupt friction increase occurs ($\approx V_R = 14.5$ m/s) and the velocity where the abrupt temperature increase starts ($= 19.1$ m/s) do not coincide with each other.

To further investigate the effects of the interfacial temperature, we also measured the friction coefficients at $V = 10.0$, 13.2, 17.4, and 19.1 m/s at room temperature T_0 ($\approx$25 °C). In Fig. 3(b), the temperature rise during the successive experiments is plotted against the difference of the friction coefficient at respective velocities between the successive experiments and those conducted separately at room temperature. As demonstrated, the friction coefficient changes little with the interfacial temperature ($\Delta\mu \sim 0.1$) in spite of $\approx$35 °C increase.

From these results, we conclude that the interfacial temperature does not trigger the abrupt friction increase even though the temperature is strongly affected by the friction-induced heat generated at the interface.

We then consider the deformation behavior of the gel. To facilitate observation, a grid was drawn on a part of the side face of the gel. Figures 4(a) and 4(e) display the snapshots at $V = 10.0$ m/s (below V_R) and 19.1 m/s (above V_S), respectively. At $V = 10.0$ m/s, the deformation of the gel is moderate and almost symmetric about the center of the

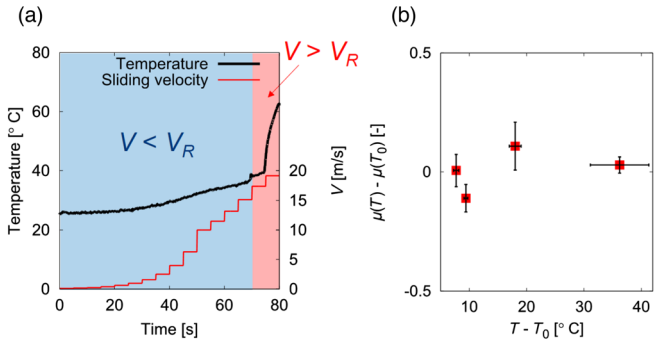

FIG. 3. (a) Sliding velocity history and the resulting evolution of the interfacial temperature during the successive friction experiments. (b) The relationship between the temperature rise during the successive experiments and the difference in the friction coefficient for the respective sliding velocities between the separate experiments at room temperature and successive ones.

contact region. In contrast, at $V = 19.1$ m/s, a bump appears on the right side of the contact region; thus, the deformation becomes highly asymmetric. The mechanism for this transition can be explained as follows: the elastic deformation is always mediated by the elastic waves. During small sliding velocities ($V < V_R$), all types of waves are transmitted downstream and upstream, and the symmetric deformation is obtained. However, at the intersonic sliding velocities ($V > V_S$), the Rayleigh and secondary waves are only transmitted downstream (clockwise direction); thus, leading to the accumulation of deformation in the right side of the contact region. It is important to note that the primary wave propagates much faster (~ km/s) than the other two (~10 m/s) and it is still transmitted in all directions.

The competition between the sliding velocity and the wave velocities has another impact on the deformation of the gel. In Figs. 4(b) and 4(f), the profiles of the gel are compared with (highlighted in green lines) and without (red lines) contact of the indenter at $V = 10.0$ and 19.1 m/s, respectively. When the sliding velocity is smaller than V_R, the deformation is observed inside and outside the contact region. As a result, the gel smoothly enters the inlet (left edge), which is similar to the Hertzian contact [29]. In contrast, when the sliding velocity exceeds V_S, almost no deformation is observed before the contact region.

As a consequence of the absence of deformation, a sharp kink is formed at the left edge of the contact region. If there is a kink, concentration of the contact pressure and breakdown of the oil film are expected. To confirm this, we performed *in situ* photoelasticity observations. Figures 4(c) and 4(g) show the corresponding snapshots. During subsonic sliding contact [$V = 10.0$ m/s, Fig. 4(c)], optical fringes similar to the Hertzian contact appear, though they are slightly deformed due to the additional frictional stress. This means that the contact pressure develops smoothly without singularity at the inlet. On the other hand, at $V = 19.1$ m/s [Fig. 4(g)], completely different fringes appear. In particular, the pattern at the left edge is similar to the frictionless contact between a rigid flat punch and a semi-infinite solid, accompanying a singular pressure field due to the edge contact [29].

These differences in the contact mode greatly affect the frictional behavior; in the subsonic regime, the contact pressure develops smoothly at the inlet and the entrainment of the oil film is maintained [see Fig. 4(d)]. In contrast, in the intersonic regime, the singular contact pressure breaks the oil film; thus, resulting in starved lubrication at the frictional interface [Fig. 4(h)].

Let us explain the abnormal deformation and photoelastic fringes above V_S with a theoretical model: the relationship between the vertical surface displacement $w(x)$ and the contact pressure distribution $p(x)$ can be described by the following equation [29]:

$$p(x) + \frac{\lambda}{\pi}\int_a^b \frac{p(s)}{x-s}ds = \alpha w'(x), \tag{2}$$

where (a, b) is the contact region and $w'(x)$ is the derivative of the surface displacement with respect to x. Here, the steady state condition is considered. The coefficients λ and α in the intersonic condition are given as,

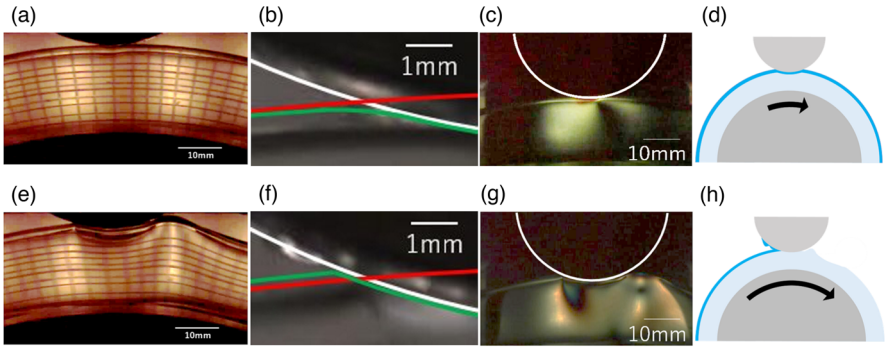

FIG. 4. Frictional behavior in the sub-Rayleigh [$V = 10.0$ m/s $< V_R$, (a)–(d)] and the intersonic [$V = 19.1$ m/s $> V_S$, (e)–(h)] regimes. (a),(d) Deformation of the gel, (b),(f) surface profiles without (red line) and with (green line) the sliding contact (the outlines of the indenter are also highlighted in white), (c),(g) photoelastic fringes, and (d),(h) the schematic of the lubricating oil film behavior.

$$\lambda = \frac{M_S^2(2-M_S^2)(2-M_S^2-2\mu\sqrt{M_S^2-1})}{4M_S^2\sqrt{M_S^2-1}+\mu\{(2-M_S^2)^3+8(M_S^2-1)\}},$$
$$\alpha = \frac{G\{(2-M_S^2)^4+16(M_S^2-1)\}}{4M_S^2\sqrt{M_S^2-1}+\mu\{(2-M_S^2)^3+8(M_S^2-1)\}}, \quad (3)$$

where $M_S = V/V_S$ is the secondary (transversal) Mach number, G is the shear modulus, and μ is the friction coefficient [the shear traction is given as $q(x) = \mu p(x)$]. We also assume that $M_P = V/V_P \ll 1$ due to the incompressibility of the gel. Details on the derivation of the coefficients are explained in the Supplemental Material [30].

The solution for $p(x)$ within the contact region is obtained as follows [29]:

$$p(x) = \frac{|\lambda|}{\sqrt{1+\lambda^2}}\frac{C}{\pi\sqrt{(x-a)(b-x)}}\left(\frac{x-a}{b-x}\right)^{\gamma} + \frac{\alpha w'(x)}{1+\lambda^2} - \frac{\alpha\lambda}{1+\lambda^2}\frac{1}{\pi\sqrt{(x-a)(b-x)}}\left(\frac{x-a}{b-x}\right)^{\gamma} \times \int_a^b \sqrt{(s-a)(b-s)}\left(\frac{b-s}{s-a}\right)^{\gamma}\frac{w'(s)}{x-s}ds, \quad (4)$$

where $C = \int_a^b p(x)dx$ and $\gamma = \tan^{-1}(1/\lambda)/\pi$. During contact between the two cylinders (with the radius R_1 and R_2), the prescribed surface deformation is $w'(x) = -x/R$ [$R = R_1R_2/(R_1+R_2)$]. The contact edge positions a and b can be determined only if $p(b) = 0$ and $C = F_N/W$ are satisfied (otherwise, the calculation does not converge). To compare the results with the experiments, we applied experimental values of $V = 19.1$ m/s and $\mu = 3.25$. The calculated contact pressure distribution is plotted in Fig. 5(a). By observing this, the distribution is highly asymmetric about the central axis ($x = 0$), and the local pressure develops sharply at the inlet ($x/R \approx -0.5$). This edgelike contact is similar to a flat punch [29] and is consistent with the photoelastic observations. Several features are noted: the pressure profile has a simple form at $V = \sqrt{2}V_S$; $p(x) = -2G/[(1+\mu)R]x$ and $(a,b) = [-\sqrt{(1+\mu)F_NR/(GW)}, 0]$. In addition, from the numerical investigations at $V_S < V < \sqrt{2}V_S$, there seems to exist no steady state solution for a positive λ [or $\mu < (2-M_S^2)/(2\sqrt{M_S^2-1})$]. We believe that this is the first theoretical solution for the intersonic sliding contact and it can be obtained only when the friction is considered.

On the other hand, the contact pressure below V_R is similar to the Hertzian contact in the static condition; the solution in the subsonic condition is given by Eqs. (4) and (5):

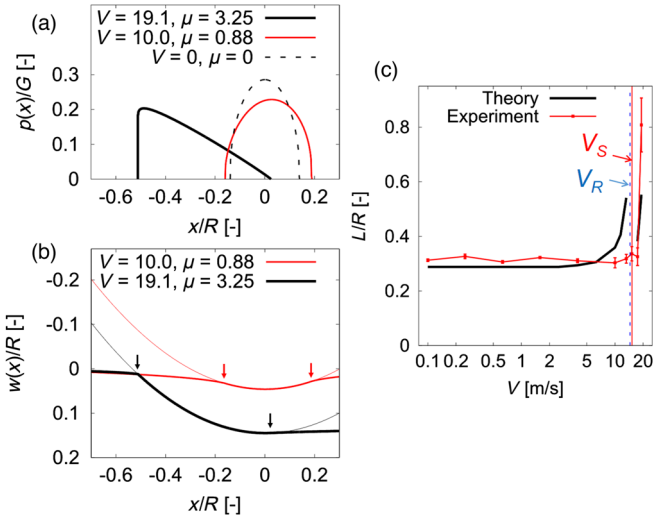

FIG. 5. (a) Contact pressure distribution at $V = 19.1$ m/s and $\mu = 3.25$, $V = 10.0$ m/s and $\mu = 0.88$, and $V = 0$ m/s and $\mu = 0$. (b) Vertical displacement at the surface for $V = 10.0$ m/s and $\mu = 0.88$, and $V = 19.1$ m/s and $\mu = 3.25$. Thin solid lines and arrows denote the indenter profiles and the contact edge positions, respectively. (c) Sliding velocity—contact length curves.

$$\lambda = \frac{1}{\mu}\frac{M_S^2}{2-M_S^2-2\sqrt{1-M_S^2}},$$
$$\alpha = \frac{G}{\mu}\frac{(2-M_S^2)^2-4\sqrt{1-M_S^2}}{2-M_S^2-2\sqrt{1-M_S^2}}. \quad (5)$$

Figure 5(a) also plots the contact pressure distribution in the subsonic ($V = 10.0$ m/s and $\mu = 0.88$) and static ($V = 0$ m/s and $\mu = 0$) conditions. It is interesting to see that the contact length becomes larger for an increased V due to the inertia-induced softening. In addition, the contact region is shifted to the right due to the frictional stress.

From Eq. (2) with the obtained contact pressure, the deformation profiles outside the contact region both for subsonic and intersonic conditions can be calculated. In Fig. 5(b), the vertical surface displacement $w(x)$ at $V = 10.0$ and 19.1 m/s are plotted. As demonstrated, the profile has a kink at the left edge ($x/R \approx -0.5$) at $V = 19.1$ m/s, while it has a smooth shape at $V = 10.0$ m/s, which is consistent with the experimental observations [see Figs. 4(b) and 4(f)]. In Fig. 5(c), the contact length $L = b - a$ is plotted as a function of V (and corresponding μ, obtained by the experiments) and compared with the experiments. At small sliding velocities, the theoretical value is almost constant and is in reasonable agreement with the experimental ones. On the other hand, as V approaches V_R, it increases abruptly and starts to deviate from the experimental ones. The reason for this deviation might be due to the viscous damping of the samples (in fact, a slight increase is recognized for the experimental values just below V_R). In contrast, above V_S, a rapid growth was observed in theory and during the

experiments. It is important to note here that a solution cannot be found at $V = 15.1$ m/s ($V_R < V < V_S$); the existence of a steady state solution should be investigated in the future.

We experimentally investigated the subsonic to intersonic transition in sliding friction by using silicone gel as a soft solid. As a result, we successfully observed an abrupt increase in the friction and abnormal deformation of the gel when the sliding velocity exceeds its secondary wave velocity. We also observed a transition in the contact pressure distributions, indicating that the propagation of the elastic waves play an essential role in intersonic friction. However, several problems remain to be solved: observation of fracture or damage processes, application of the elastohydrodynamic lubrication theory to intersonic friction, and the stability analyses around the steady state are other important issues. These topics need to be studied in the future.

T. Y. acknowledges H. Sakaguchi and S. Hirano for their important suggestions. This work was supported by JSPS KAKENHI Grants No. JP16H06478 and No. JP18K03565. We would like to thank Editage [31] for English language editing.

[1] B. N. J. Persson, *Sliding Friction: Theory and Applications* (Springer, Heidelberg, 1998).
[2] V. L. Popov, *Contact Mechanics and Friction: Physical Principles and Applications* (Springer-Verlag Berlin Heidelberg, 2017), 2nd ed.
[3] J. H. Dieterich, J. Geophys. Res. Solid Earth **84**, 2161 (1979).
[4] M. L. Blanpied, T. E. Tullis, and J. D. Weeks, Geophys. Res. Lett. **14**, 554 (1987).
[5] B. D. Kilgore, M. L. Blanpied, and J. H. Dieterich, Geophys. Res. Lett. **20**, 903 (1993).
[6] H. Yoshizawa, Y.-L. Chen, and J. Israelachvili, Wear **168**, 161 (1993).
[7] T. Baumberger, F. Heslot, and B. Perrin, Nature (London) **367**, 544 (1994).
[8] E. Gnecco, R. Bennewitz, T. Gyalog, Ch. Loppacher, M. Bammerlin, E. Meyer, and H.-J. Guntherodt, Phys. Rev. Lett. **84**, 1172 (2000).
[9] T. Baumberger, C. Caroli, and O. Ronsin, Phys. Rev. Lett. **88**, 075509 (2002).
[10] R. Tadmor, J. Janik, J. Klein, and L. J. Fetters, Phys. Rev. Lett. **91**, 115503 (2003).
[11] G. Di Toro, D. L. Goldsby, and T. E. Tullis, Nature (London) **427**, 436 (2004).
[12] S. M. Rubinstein, G. Cohen, and J. Fineberg, Nature (London) **430**, 1005 (2004).
[13] T. Yamaguchi, S. Ohmata, and M. Doi, J. Phys. Condens. Matter **21**, 205105 (2009).
[14] M. Morishita, M. Kobayashi, T. Yamaguchi, and M. Doi, J. Phys. Condens. Matter **22**, 365104 (2010).
[15] T. Yamaguchi, M. Morishita, M. Doi, T. Hori, H. Sakaguchi, and J.-P. Ampuero, J. Geophys. Res. **116**, B12306 (2011).
[16] T. Yamaguchi, Y. Sawae, and S. M. Rubinstein, Extreme Mech. Lett. **9**, 331 (2016).
[17] T. Baumberger and C. Caroli, Adv. Phys. **55**, 279 (2006).
[18] A. E. Norton, *Lubrication* (McGraw-Hill, New York, 1942).
[19] K. A. Grosch, Proc. R. Soc. A **274**, 21 (1963).
[20] B. N. J. Persson, J. Chem. Phys. **115**, 3840 (2001).
[21] L. M. Milne-Thomson, *Theoretical Aerodynamics* (Dover Publications, New York, 2012).
[22] F. X. Passelègue, A. Schubnel, S. Nielsen, H. S. Bhat, and R. Madariaga, Science **340**, 1208 (2013).
[23] K. Xia, A. J. Rosakis, and H. Kanamori, Science **303**, 1859 (2004).
[24] J. D. Cole and J. H. Huth, ASME J. Appl. Mech. **25**, 433 (1958).
[25] J. W. Craggs and A. M. Roberts, J. Appl. Mech. **34**, 207 (1967).
[26] H. G. Georgiadis and J. R. Barber, J. Elast. **31**, 141 (1993).
[27] H. G. Georgiadis and J. R. Barber, J. Appl. Mech. **60**, 772 (1993).
[28] J. R. Barber, J. Appl. Mech. **63**, 245 (1996).
[29] K. L. Johnson, *Contact Mechanics* (Cambridge University Press, Cambridge, England, 1985).
[30] See the Supplemental Material at http://link.aps.org/supplemental/10.1103/PhysRevLett.124.238001 for the measurement of local sliding velocities in the intersonic sliding condition and the derivation of Green's functions.
[31] www.editage.com.